Supporting Information

Multifunctional Electrocatalysis on Porous N-Doped $NiCo_2O_4$@C Nanonetwork

Yuan Ha, Lingxia Shi, Xiaoxiao Yan, Ziliang Chen, Yunpeng Li, Wei Xu, Renbing Wu*

Department of Materials Science, Fudan University, Shanghai 200433, China

*Email address: rbwu@fudan.edu.cn

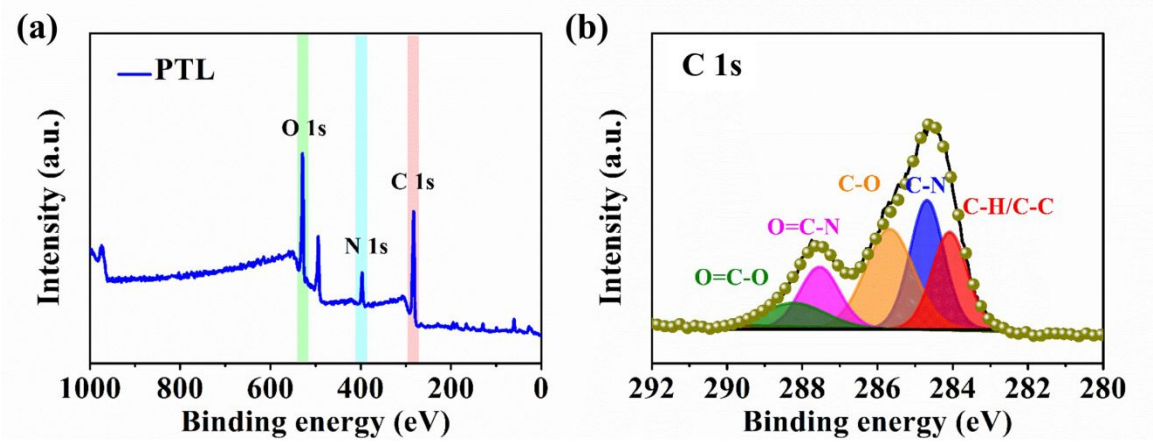

Figure S1. (a) XPS survey spectra of PTL; (b) corresponding high-resolution XPS spectra of the C 1s.[S1, S2]

Note: the high-resolution XPS spectra in Figure S1b can be fitted into five peaks at284.1, 284.7, 285.6, 287.5 and 288.3 eV corresponding to C-H/C-C, C-N, C-O, O=C-N and O=C-O, respectively, which is also similar to previous reports. [S1,S2]

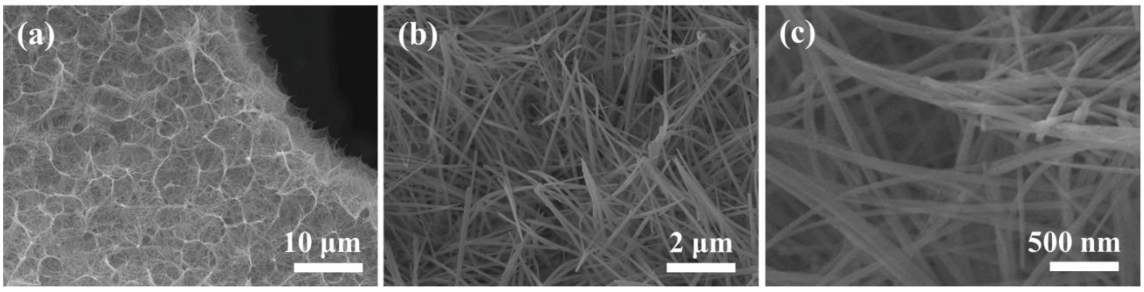

Figure S2. (a-c) FESEM images of $NiCo_2O_4$@PTL@NF precursor.

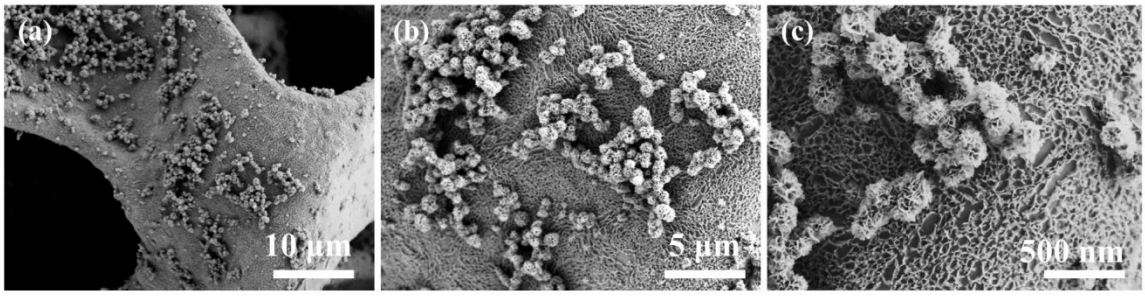

Figure S3. (a-c) FESEM images of $NiCo_2O_4$ structures directly grown on nickel foam without PTL nanofilm ($NiCo_2O_4$@NF).

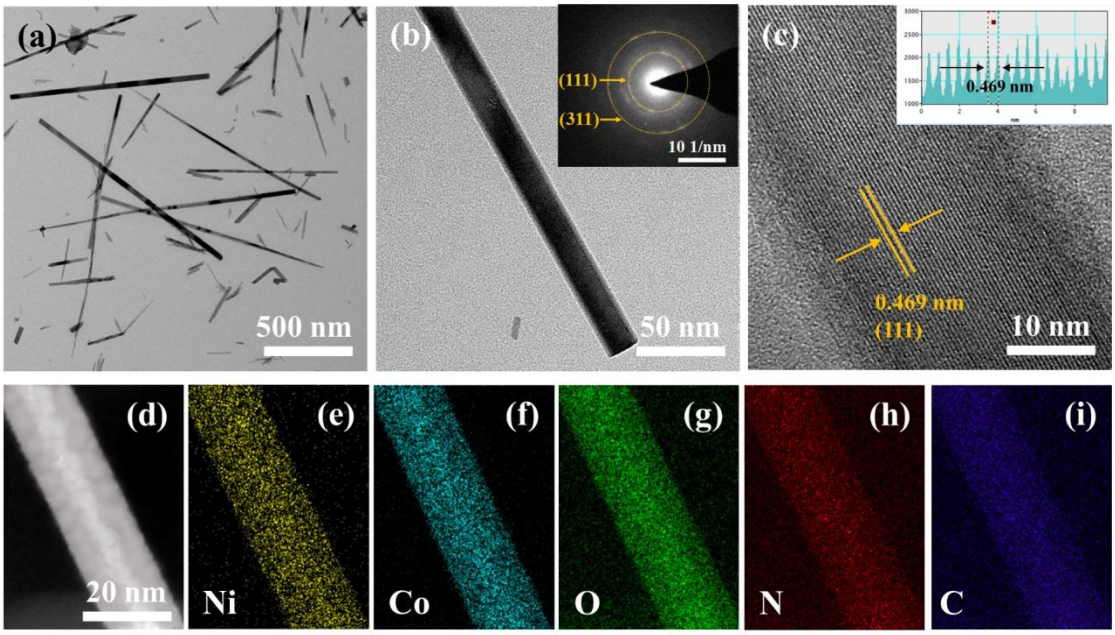

Figure S4. $NiCo_2O_4$@PTL precursor: (a) TEM image; (b) magnifed TEM image; (c) HRTEM image, the inset in Figure S4b showing the corresponding SAED and the lattice spacing corresponding to the selected areas in panel (Figure S4c); (d) HAADF-STEM image and (e-i) EDS elemental mapping images of $NiCo_2O_4$@PTL precursor.

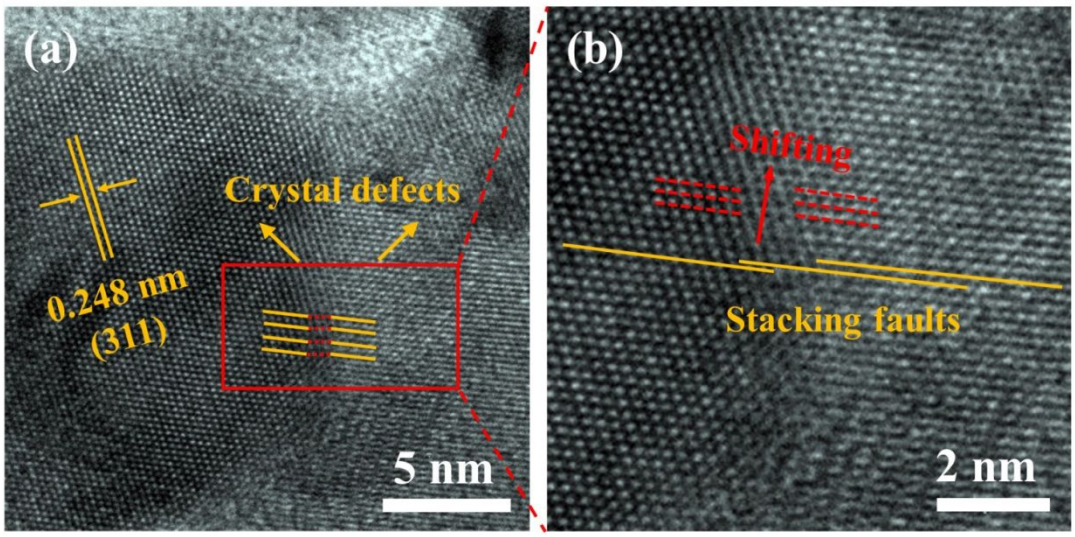

Figure S5. N-$NiCo_2O_4$@C: (a) HRTEM image (b) magnified HRTEM image rocorded from red square in (a).

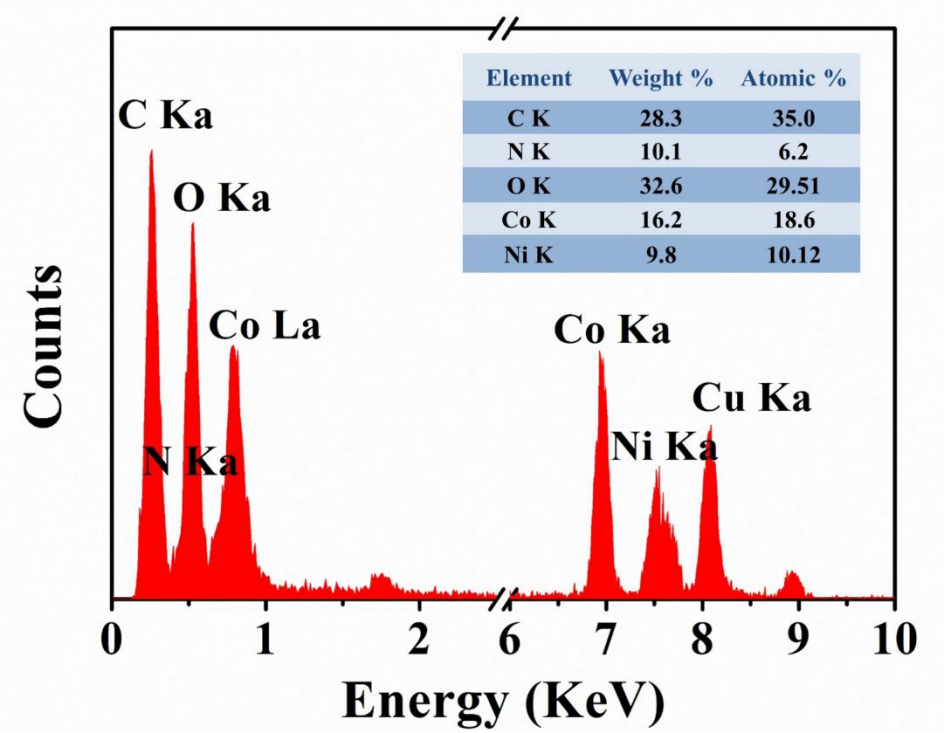

Figure S6. EDS results of N-$NiCo_2O_4$@C. The EDS elemental results confirm that the corresponding Co/Ni ratio of synthesized N-$NiCo_2O_4$@C are close to the chemical formula for spinal $NiCo_2O_4$.

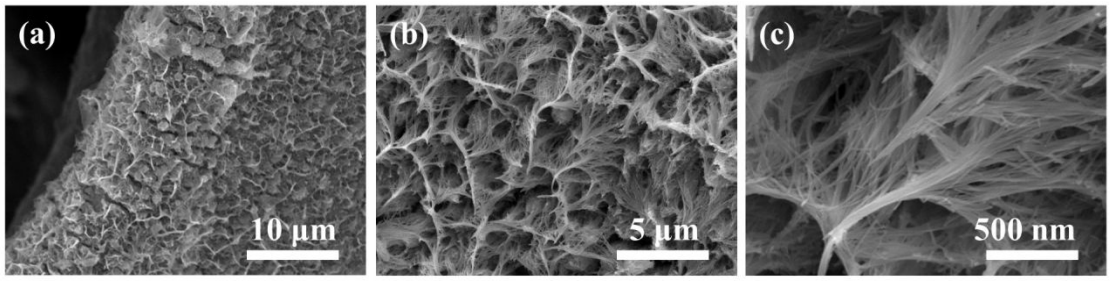

Figure S7. (a-c) FESEM images of N-$NiCo_2O_4$@C@NF after 15 min high-powered ultrasonication.

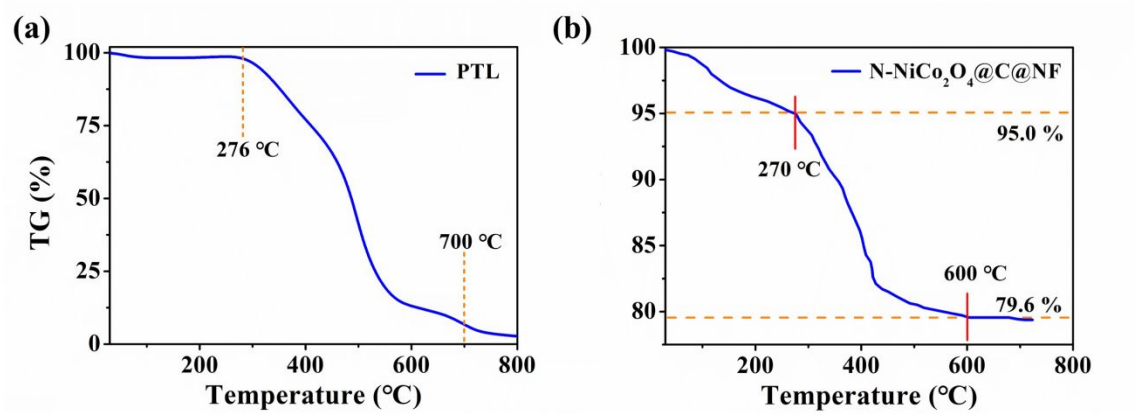

Figure S8. TGA curves of (a) PTL and (b) N-$NiCo_2O_4$@C@NF under air atmosphere at a heating rate of 10 ℃ min^{-1}.

The carbon content in the N-$NiCo_2O_4$@C composites can be evaluated from the TGA results as following (Noted that the products were shaved from NF before TGA testing):

Firstly, the TG curve of PTL shows a sharp mass decrease from 276 to 700℃, corresponding to the decomposition of PTL, whereas the N-$NiCo_2O_4$@C exhibits a slow mass loss before 270 ℃, caused by the removal of water and hydroxy groups probably adsorbed on the surface of the composite. The continuous weight loss from 270 ℃ to 600 ℃ is ascribed to the burning of PTL-carbon since the temperature of thermal decomposition. As for the N-$NiCo_2O_4$@C, a weight loss of 15.4 % was found after heating 232 ℃, which could be ascribed to the combustion of PTL.

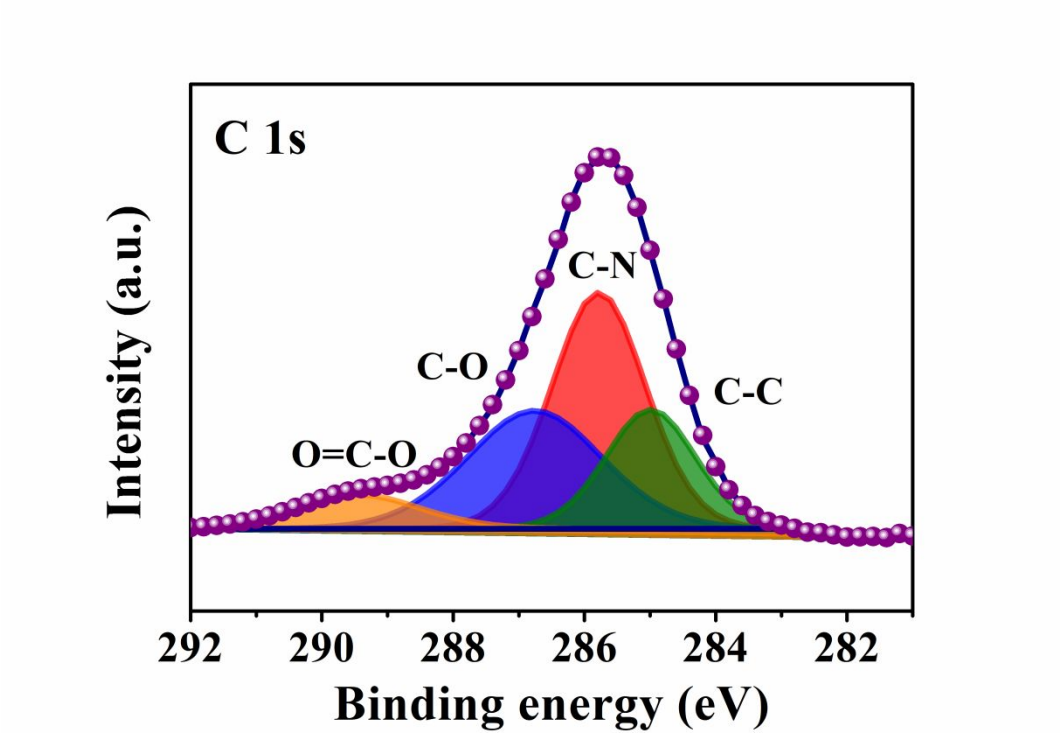

Figure S9. High-resolution XPS spectra of C 1s in N-$NiCo_2O_4$@C.

Element	Position (eV)	Atomic %
C 1s	284.6	7.35
N 1s	400.2	4.8
O 1s	529.8	45.22
Co 2p	779.6	16.68
Ni 2p	854.3	25.95

Figure S10. Quantitative analysis of the N-$NiCo_2O_4$@C based on the high-resolution XPS spectra.

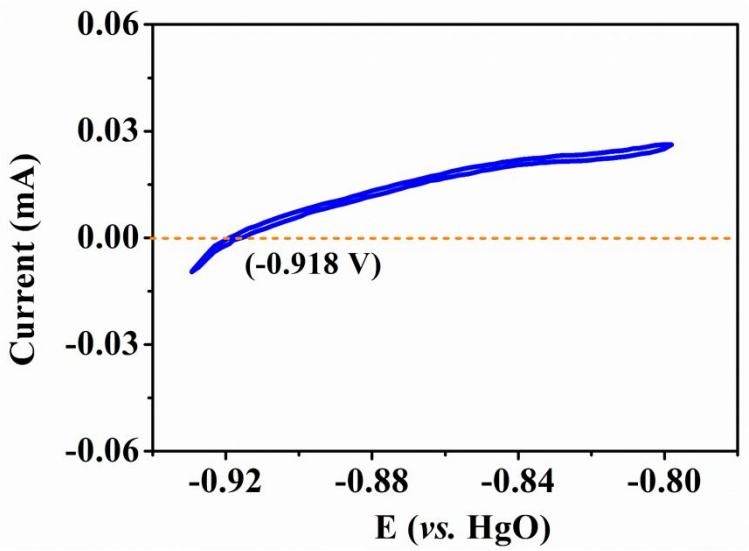

Figure S11. The CV curve at a scan rates of 1 mV s^{-1} in hydrogen-saturated 1.0 M KOH.

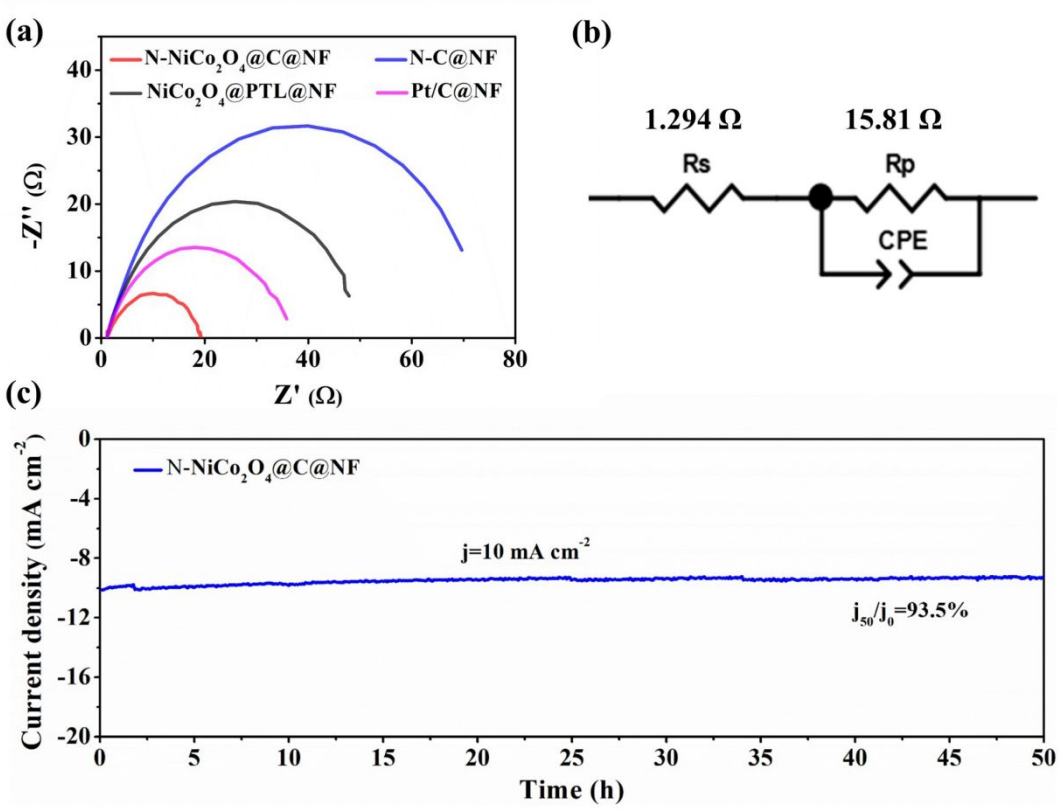

Figure S12. (a) EIS spectra of N-$NiCo_2O_4$@C@NF, $NiCo_2O_4$@PTL@NF precursor, N-C@NF and Pt/C@NF for HER; (b) corresponding equivalent circuit diagram; (c) stability test of N-$NiCo_2O_4$@C@NF under high current density for 50 h at a constant potential of −0.046 V *vs.* RHE.

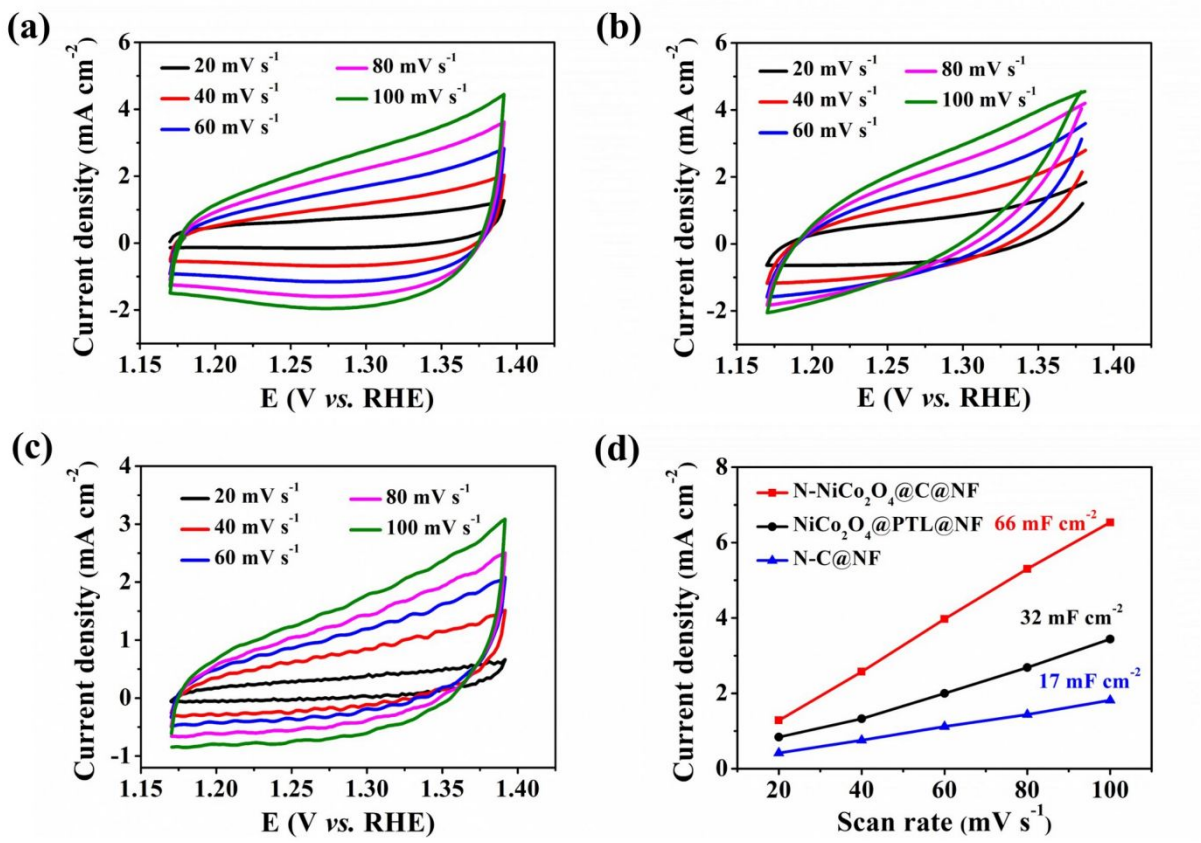

Figure S13. CV curves of (a) N-$NiCo_2O_4$@C@NF, (b) $NiCo_2O_4$@PTL@NF precursor and (c) N-C@NF at different scan rates, and (d) corresponding plots of the capacitive currents as a function of scan rate.

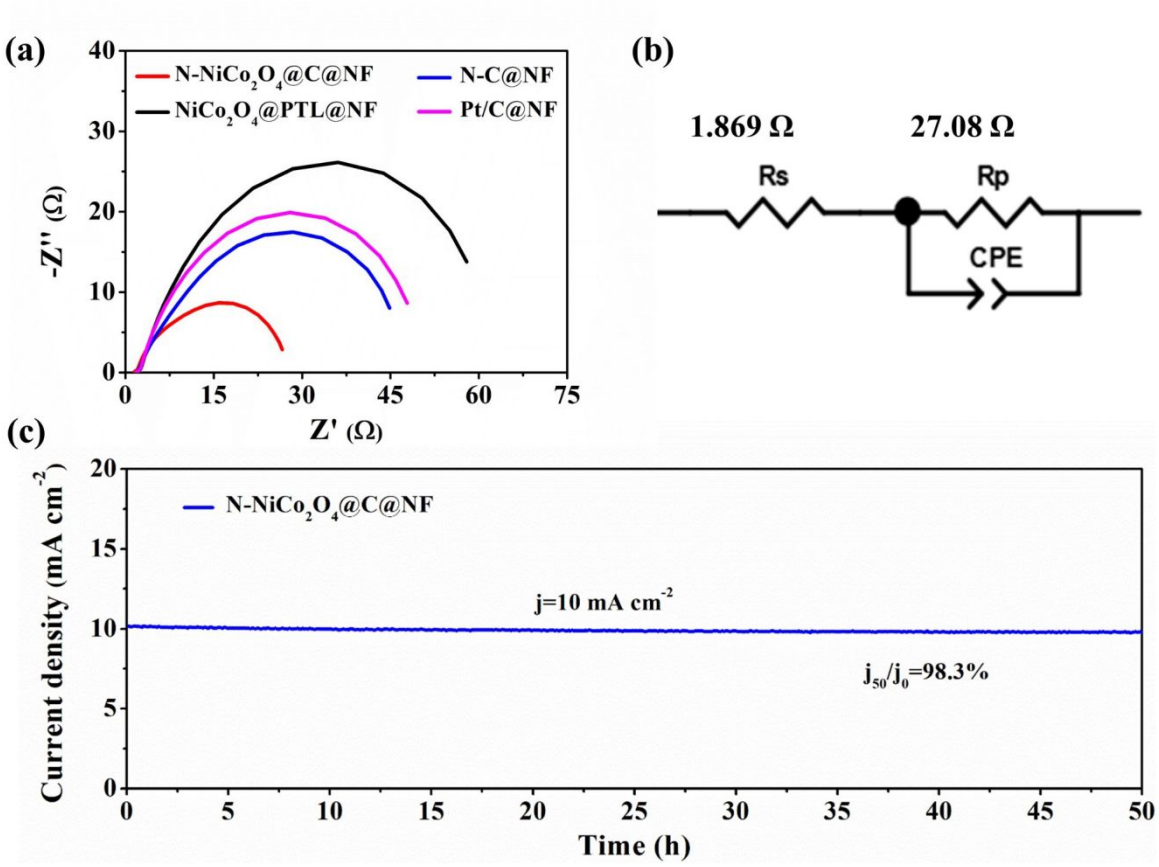

Figure S14. (a) EIS spectra of N-$NiCo_2O_4$@C@NF, $NiCo_2O_4$@PTL@NF precursor, N-C@NF and Pt/C@NF for OER; (b) corresponding equivalent circuit diagram; (c) stability test of N-$NiCo_2O_4$@C@NF at a constant potential of −1.46 V *vs.* RHE for 50 h.

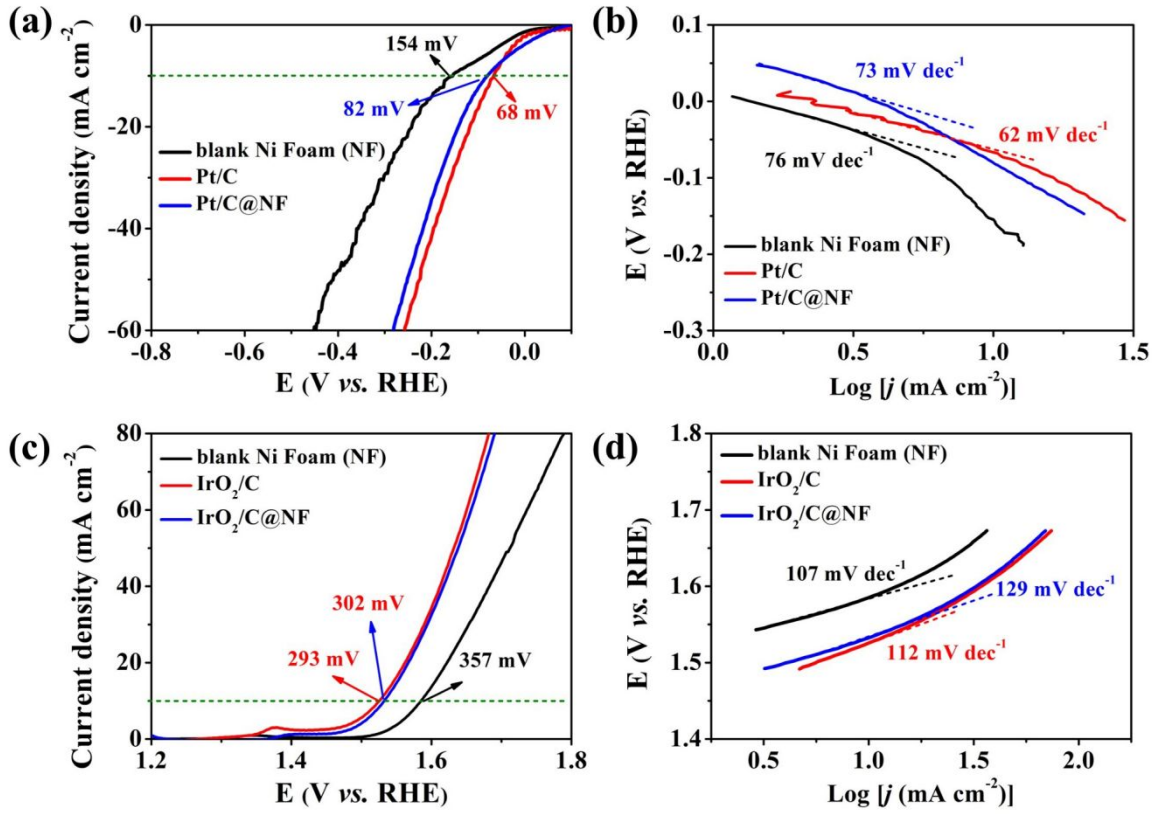

Figure S15. HER and OER performance of blank Ni foam, pure Pt/C and Pt/C@NF or pure IrO_2/C and IrO_2/C@NF. (a) HER LSV curves, (b) HER Tafel plots, and (c) OER LSV curves, (d) HER Tafel plots.

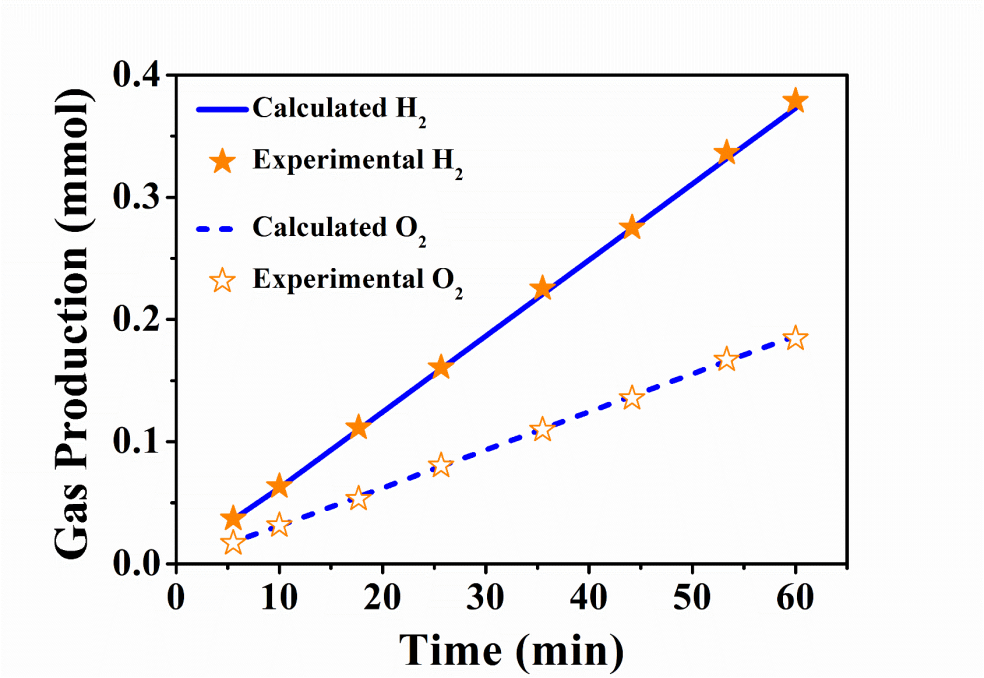

Figure S16. The measured and theoretical yields of O_2 and H_2 over time during electrolysis of N-$NiCo_2O_4$@C@NF at the current density of 10 mA cm^{-2}.

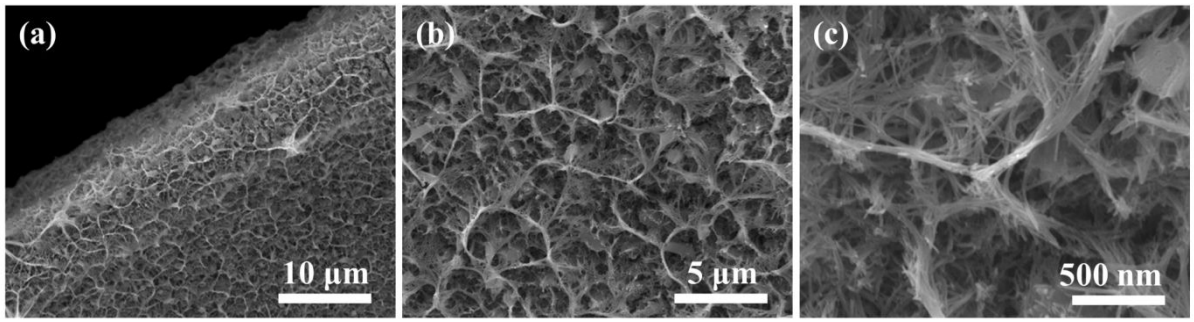

Figure S17. (a-c) FESEM images of the N-$NiCo_2O_4$@C@NF after cycling test for water splitting.

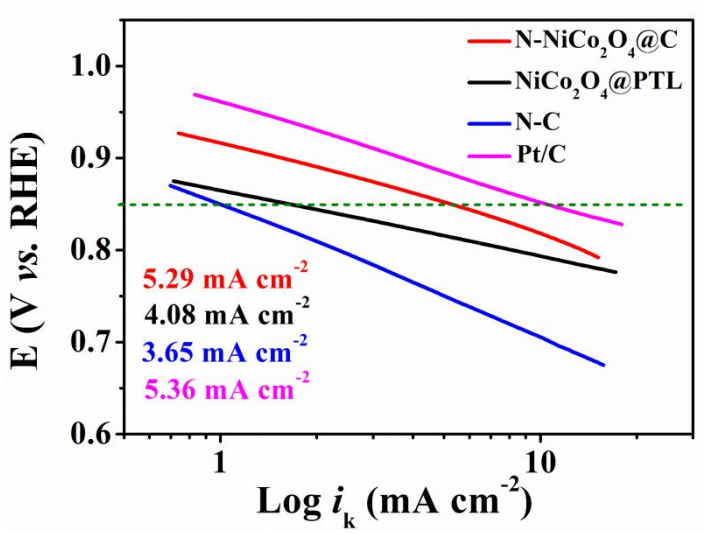

Figure S18. The ORR Tafel plots of N-$NiCo_2O_4$@C, $NiCo_2O_4$@PTL, N-C, and Pt/C catalysts in 0.1 M KOH.

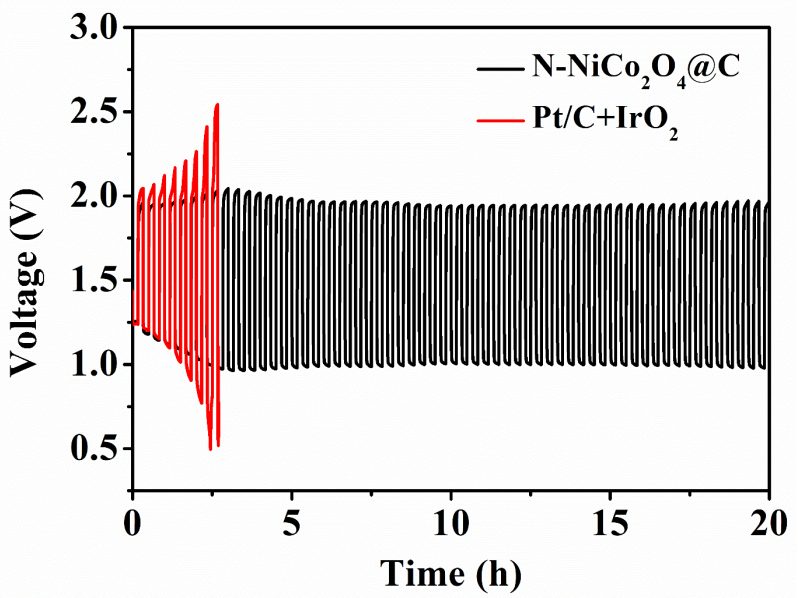

Figure S19. Galvanostatic charge and discharge test of Zn-air battery based on N-$NiCo_2O_4$@C and Pt/C+IrO_2 at current density of 10 mA cm^{-2}.

Table S1. Comparison of the electrocatalytic activity of N-$NiCo_2O_4$@C@NF and the reported catalysts for HER in 1.0 M KOH.

Catalyst	Current density (*j*)	overpotential	Ref.
N-$NiCo_2O_4$@C@NF	**10 mA cm^{-2}**	**42 mV**	**This work**
$NiCo_2O_4$ hollow microcuboids	10 mA cm^{-2}	110 mV	(S3)
NiCo/$NiCoO_x$/NF	10 mA cm^{-2}	155 mV	(S4)
$Fe_{11\%}$-NiO/NF	10 mA cm^{-2}	88 mV	(S5)
$Ni_xCo_{3-x}S_4/Ni_3S_2$/NF	10 mA cm^{-2}	136 mV	(S6)
Co_4Ni_1P NTS	10 mA cm^{-2}	192 mV	(S7)
$NiCo_2O_4$NA/CC	10 mA cm^{-2}	175 mV	(S8)
$Ni_{0.82}Co_{0.18}O$@C /NF	10 mA cm^{-2}	194 mV	(S9)
NiCoFe LTHs/CFC	10 mA cm^{-2}	200 mV	(S10)
NiCo-PBA/NF	10 mA cm^{-2}	62 mV	(S11)
$NiCo_2S_4$	10 mA cm^{-2}	80 mV	(S12)
3D Se-(NiCo)S_x/$(OH)_x$ nanosheets	10 mA cm^{-2}	103 mV	(S13)
$NiCo_2O_4$@$CoMoO_4$/NF	10 mA cm^{-2}	121 mV	(S14)
NiCoP/CC	10 mA cm^{-2}	62 mV	(S15)
$Ni_{0.5}Co_{0.5}$ nanowire	10 mA cm^{-2}	36 mV	(S16)

Table S2. Comparison of the electrocatalytic activity of N-$NiCo_2O_4$@C@NF and the reported catalysts for OER in 1.0 M KOH.

Catalyst	Current density (*j*)	overpotential	Ref.
N-$NiCo_2O_4$@C@NF	**10 mA cm^{-2}**	**242 mV**	**This work**
$NiCo_2O_4$ hollow microcuboids	10 mA cm^{-2}	270 mV	(S3)
Co_4Ni_1P NTS	10 mA cm^{-2}	245 mV	(S7)
$Ni_{0.82}Co_{0.18}O$@C /NF	10 mA cm^{-2}	330 mV	(S9)
NiCoFe LTHs/CFC	10 mA cm^{-2}	239 mV	(S10)
NiCo-PBA/NF	10 mA cm^{-2}	200 mV	(S11)
$NiCo_2S_4$	10 mA cm^{-2}	243 mV	(S12)
3D Se-(NiCo)S*x*/(OH)*x* nanosheets	10 mA cm^{-2}	155 mV	(S13)
$MnFe_2O_4/NiCo_2O_4$	10 mA cm^{-2}	330 mV	(S17)
NiCo/NLG-270	10 mA cm^{-2}	340 mV	(S18)
$NiCo_2S_4$/N-CNT	10 mA cm^{-2}	370 mV	(S19)
NiCo/PFC aerogels	10 mA cm^{-2}	400 mV	(S20)
$NiCo_2O_4$/Graphene	10 mA cm^{-2}	440 mV	(S21)
NiCoP/C nanoboxes	10 mA cm^{-2}	330 mV	(S22)
$Ni_xCo_{3-x}O_4$	10 mA cm^{-2}	337 mV	(S23)

Table S3. The two-electrode system for overall water electrolysis in 1.0 M KOH.

Catalyst	Current density (*j*)	Potential	Ref.
N-$NiCo_2O_4$@C@NF	**10 mA cm^{-2}**	**1.43 V**	**This work**
$NiCo_2O_4$ hollow microcuboids	10 mA cm^{-2}	1.65 V	(S3)
$Ni_xCo_{3-x}S_4/Ni_3S_2$/NF	10 mA cm^{-2}	1.53 V	(S6)
Co_4Ni_1P nanotubes	10 mA cm^{-2}	1.59 V	(S7)
$NiCo_2O_4$NA/CC	10 mA cm^{-2}	1.68 V	(S8)
$Ni_{0.82}Co_{0.18}O$@C /NF	10 mA cm^{-2}	1.42 V	(S9)
NiCoFe LTHs/CFC	10 mA cm^{-2}	1.55 V	(S10)
NiCo-PBA/NF	10 mA cm^{-2}	1.49 V	(S11)
$NiCo_2S_4$	10 mA cm^{-2}	1.58 V	(S12)
3D Se-(NiCo)S_x/$(OH)_x$ nanosheets	10 mA cm^{-2}	1.60 V	(S13)
$NiCo_2O_4$@$CoMoO_4$/NF	10 mA cm^{-2}	1.55 V	(S14)
$NiCo_2P_x$	10 mA cm^{-2}	1.61 V	(S24)
$NiCo_2O_4/Ni_2P$/N	10 mA cm^{-2}	1.59 V	(S25)
NiCoP/NF	10 mA cm^{-2}	1.58 V	(S26)
NiFe/$NiCo_2O_4$/Ni	10 mA cm^{-2}	1.67 V	(S27)

Table S4. Summary of reported half-wave potential ($E_{1/2}$) and diffusion-limited current density (J_L) values at 1600 rpm for NiCo-based Electrocatalysts. Noted all data are obtained in 0.1 M in an O_2 saturated 0.1 M KOH solution at a rotation rate of 1600 rpm.

Catalyst	E_{onset} (*vs.* RHE)	$E_{1/2}$ (*vs.* RHE)	J_L(mA cm^{-2})	Ref.
N-$NiCo_2O_4$@C@NF	**0.91 V**	**0.81 V**	**5.2**	**This work**
$NiCo_2S_4$/N-CNT	0.93 V	0.80 V	3.4	(S19)
$NiCo_2S_4$-CNT	0.84 V	0.69 V	2.7	(S19)
$NiCo_2S_4$	0.77 V	0.64 V	2.2	(S19)
NiCo/PFC aerogels	0.92 V	0.79 V	5.8	(S20)
$NiCo_2O_4$/Graphene	0.87 V	0.69 V	3.4	(S21)
$NiCo_2O_4$ NWs	0.80 V	0.76 V	6.0	(S28)
macroporous $NiCo_2O_4$	0.83 V	0.78 V	1.6	(S29)
$NiCo_2O_4$/rGO	0.91 V	0.78 V	1.6	(S30)
$NiCo_2O_4$/graphene foam	0.9 V	0.86 V	6.2	(S31)
1D-spinel $NiCo_2O_4$	0.84 V	0.78 V	6.0	(S32)
NiCo@N-C	0.96 V	0.81 V	6.5	(S33)
$NiCo_2S_4$@N/S-rGO	0.88 V	0.80 V	4.3	(S34)
$NiCo_2O_4$/HCS	0.90 V	0.78 V	5.8	(S35)
$NiCo_2O_4$/Co,N-CNTs NCs	0.92 V	0.86 V	5.2	(S36)

REFERENCES

(S1) Ha, Y.; Yang, J.; Tao, F.; Wu, Q.; Song, Y.; Wang, H.; Zhang, X.; Yang, P. Phase-Transited Lysozyme as a Universal Route to Bioactive Hydroxyapatite Crystalline Film. *Adv. Funct. Mater.* **2018**, *28*, 1704476.

(S2) Ha, Y.; Shi, L.; Chen, Z.; Wu, R. Phase-Transited Lysozyme-Driven Formation of Self-Supported Co_3O_4@C Nanomeshes for Overall Water Splitting. *Adv. Sci.* **2019**, *6*, 1900272.

(S3) Gao, X.; Zhang, H.; Li, Q.; Yu, X.; Hong, Z.; Zhang, X.; Liang, C.; Lin, Z. Hierarchical $NiCo_2O_4$ Hollow Microcuboids as Bifunctional Electrocatalysts for Overall Water-Splitting. *Angew. Chem. Int. Ed.* **2016**, *55*, 6290–6294.

(S4) Yan, X.; Li, K.; Lyu, L.; Song, F.; He, J.; Niu, D.; Liu, L.; Hu, X.; Chen, X. From Water Oxidation to Reduction: Transformation from $Ni_xCo_{3-x}O_4$ Nanowires to NiCo/$NiCoO_x$ Heterostructures. *ACS Appl. Mater. Interfaces* **2016**, *8*, 3208–3214.

(S5) Wu, Z.; Zou, Z.; Huang, J.; Gao, F. Fe-Doped NiO Mesoporous Nanosheets Array for Highly Efficient Overall Water Splitting. *J. Catal.* **2018**, *358*, 243–252.

(S6) Wu, Y.; Liu, Y.; Li, G; Zou, X.; Lian, X.; Wang, D.; Sun, L.; Asefa, T.; Zou, X. Efficient Electrocatalysis of Overall Water Splitting by Ultrasmall Ni_xCo_{3}-$_xS_4$ Coupled Ni_3S_2 Nanosheet Arrays. *Nano Energy* **2017**, *35*, 161–170.

(S7) Yan, L.; Cao, L.; Dai, P.; Gu, X.; Liu, D.; Li, L.; Wang, Y.; Zhao, X. Metal-Organic Frameworks Derived Nanotube of Nickel-Cobalt Bimetal Phosphides as Highly Efficient Electrocatalysts for Overall Water Splitting. *Adv. Funct. Mater.* **2017**, *27*, 1703455.

(S8) Liu, D.; Lu, Q.; Luo, Y.; Sun, X.; Asiri, A. $NiCo_2S_4$ Nanowires Array as an Efficient Bifunctional Electrocatalyst for Full Water Splitting with Superior Activity. *Nanoscale* **2015**, *7*, 15122–15126.

(S9) Yang, H.; Chen, Z.; Hao, W.; Xu, H.; Guo, Y.; Wu, R. Catalyzing Overall Water Splitting at an Ultralow Cell Voltage of 1.42 V Via Coupled Co-doped NiO Nanosheets with Carbon. *Appl. Catal. B: Environ.* **2019**, *252*, 214–221.

(S10) Wang, A.; Xu, H.; Li, G. NiCoFe Layered Triple Hydroxides with Porous Structures as High-Performance Electrocatalysts for Overall Water Splitting. *ACS Energy Lett.* **2016**, *1*, 445–453.

(S11) Ma, L.; Zhou, B.; Tang, L.; Guo, J.; Liu, Q.; Zhang, X. Template Confined Synthesis of NiCo Prussian Blue Analogue Bricks Constructed Nanowalls as Efficient Bifunctional Electrocatalyst for Splitting Water. *Electrochim. Acta.* **2019**, *318*, 333–341.

(S12) Kang, Z.; Guo, H.; Wu, J.; Sun, X.; Zhang, Z.; Liao, Q.; Zhang, S.; Si, H.; Wu, P.; Wang, L.; Zhang, Y. Engineering an Earth-Abundant Element-Based Bifunctional Electrocatalyst for Highly Efficient and Durable Overall Water Splitting. *Adv. Funct. Mater.* **2019**, *29*, 1807031.

(S13) Hu, C.; Zhang, L.; Zhao, Z.; Li, A.; Chang, X.; Gong, J. Synergism of Geometric Construction and Electronic Regulation: 3D Se-$(NiCo)S_x/(OH)_x$ Nanosheets for Highly Efficient Overall Water Splitting. *Adv. Mater.* **2018**, *30*, 1705538.

(S14) Gong, Y.; Yang, Z.; Lin, Y.; Wang, J.; Pan, H.; Xu, Z. Hierarchical Heterostructure $NiCo_2O_4$@$CoMoO_4$/NF as an Efficient Bifunctional Electrocatalyst for Overall Water Splitting. *J. Mater. Chem. A* **2018**, *6*, 16950–16958.

(S15) Du, C.; Yang, L.; Yang, F.; Cheng, G.; Luo, W. Nest-Like NiCoP for Highly Efficient Overall Water Splitting. *ACS Catal.* **2017**, *7*, 4131–4137.

(S16) Zou, P.; Li, J.; Zhang, Y.; Liang, C.; Yang, C.; Fan, H. Magnetic-Field-Induced Rapid Synthesis of Defect-Enriched Ni-Co Nanowire Membrane as Highly Efficient Hydrogen Evolution Electrocatalyst. *Nano Energy* **2018**, *51*, 349–357.

(S17) Zhang, Y. Q.; Li, M.; Hua, B.; Wang, Y.; Sun, Y. F.; Luo, J. A Strongly Cooperative Spinel Nanohybrid as an Efficient Bifunctional Oxygen Electrocatalyst for Oxygen

Reduction Reaction and Oxygen Evolution Reaction. *Appl. Catal. B: Environ.* **2018**, *236*, 413–419.

(S18) Wang, X.; Liu, J.; Liu, Z.; Wang, W.; Luo, J.; Han, X.; Du, X.; Qiao, S.; Yang, J. Identifying the Key Role of Pyridinic-N-Co Bonding in Synergistic Electrocatalysis for Reversible ORR/OER. *Adv. Mater.* **2018**, *30*, 1800005.

(S19) Han, X.; Wu, X.; Zhong, C.; Deng, Y.; Zhao, N.; Hu, W. $NiCo_2S_4$ Nanocrystals Anchored on Nitrogen-Doped Carbon Nanotubes as a Highly Efficient Bifunctional Electrocatalyst for Rechargeable Zinc-Air Batteries. *Nano Energy* **2017**, *31*, 541–550.

(S20) Fu, G.; Chen, Y.; Cui, Z.; Li, Y.; Zhou, W.; Xin, S.; Tang, Y.; Goodenough, J. B. Novel Hydrogel-Derived Bifunctional Oxygen Electrocatalyst for Rechargeable Air Cathodes. *Nano Lett.* **2016**, *16*, 6516–6522.

(S21) Lee, D.; Kim, B.; Chen, Z. One-Pot Synthesis of a Mesoporous $NiCo_2O_4$ Nanoplatelet and Graphene Hybrid and its Oxygen Reduction and Evolution Activities as an Efficient Bi-Functional Electrocatalyst. *J. Mater. Chem. A* **2013**, *1*, 4754–4762.

(S22) He, P.; Yu, X. Y.; Lou, X. Carbon-incorporated Nickel-Cobalt Mixed Metal Phosphide Nanoboxes with Enhanced Electrocatalytic Activity for Oxygen Evolution. *Angew. Chem. Int. Ed.* **2017**, *56*, 3897–3900.

(S23) Yu, Z.; Bai, Y.; Liu, Y.; Zhang, S.; Chen, D.; Zhang, N.; Sun, K. Metal-Organic-Framework-Derived Yolk-Shell-Structured Cobalt-Based Bimetallic Oxide Polyhedron with High Activity for Electrocatalytic Oxygen Evolution. *ACS Appl. Mater. Interfaces* **2017**, *9*, 31777–31785.

(S24) Huang, C.; Ouyang, T.; Zou, Y.; Li, N.; Liu, Z. Ultrathin $NiCo_2P_x$ Nanosheets Strongly Coupled with CNTs as Efficient and Robust Electrocatalysts for Overall Water Splitting. *J. Mater. Chem. A* **2018**, *6*, 7420–7427.

(S25) Wang, L.; Gu, C.; Ge, X.; Zhang, J.; Zhu, H.; Tu, J. Anchoring Ni_2P Sheets on $NiCo_2O_4$ Nanocone Arrays as Optimized Bifunctional Electrocatalyst for Water Splitting. *Appl. Mater. Interfaces* **2017**, *4*, 1700481.

(S26) Liang, H.; Gandi, A. N.; Anjum, D. H.; Wang, X.; Schwingenschlögl, U.; Alshareef, H. N. Plasma-Assisted Synthesis of NiCoP for Efficient Overall Water Splitting. *Nano Lett.* **2016**, *16*, 7718–7725.

(S27) Xiao, C.; Li, Y.; Lu, X.; Zhao, C. Bifunctional Porous NiFe/$NiCo_2O_4$/Ni Foam Electrodes with Triple Hierarchy and Double Synergies for Efficient Whole Cell Water Splitting. *Adv. Funct. Mater.* **2016**, *26*, 3515–3523.

(S28) Jin, C.; Lu, F.; Cao, X.; Yang, Z.; Yang, R. Facile Synthesis and Excellent Electrochemical Properties of $NiCo_2O_4$ Spinel Nanowire Arrays as a Bifunctional Catalyst for the Oxygen Reduction and Evolution Reaction. *J. Mater. Chem. A* **2013**, *1*, 12170–12177.

(S29) Xiao, Y.; Hu, C.; Qu, L.; Hu, C.; Cao, M. Three-Dimensional Macroporous $NiCo_2O_4$ Sheets as a Non-Noble Catalyst for Efficient Oxygen Reduction Reactions. *Chem. Eur. J.* **2013**, *19*, 14271–14278.

(S30) Zhang, G.; Xia, B. Y.; Wang, X.; Lou, X. W. Strongly Coupled $NiCo_2O_4$-rGO Hybrid Nanosheets as a Methanol-Tolerant Electrocatalyst for the Oxygen Reduction Reaction. *Adv. Mater.* **2014**, *26*, 2408–2412.

(S31) Tong, X.; Chen, S.; Guo, C.; Xia, X.; Guo, X. Y. Mesoporous $NiCo_2O_4$ Nanoplates on Three-Dimensional Graphene Foam as an Efficient Electrocatalyst for the Oxygen Reduction Reaction. *ACS Appl. Mater. Interfaces* **2016**, *8*, 28274–28282.

(S32) Prabu, M.; Ketpang, K.; Shanmugam, S. Hierarchical Nanostructured $NiCo_2O_4$ as an Efficient Bifunctional Non-Precious Metal Catalyst for Rechargeable Zinc-air Batteries. *Nanoscale* **2014**, *6*, 3173–3181.

(S33) Fu, Y.; Yu, H. Y.; Jiang, C.; Zhang, T. H.; Zhan, R.; Li, X.; Yang, R. NiCo Alloy Nanoparticles Decorated on N-Doped Carbon Nanofibers as Highly Active and Durable Oxygen Electrocatalyst. *Adv. Funct. Mater.* **2018**, *28*, 1705094.

(S34) Liu, Q.; Jin, J.; Zhang, J. $NiCo_2S_4$@Graphene as a Bifunctional Electrocatalyst for Oxygen Reduction and Evolution Reactions. *ACS Appl. Mater. Interfaces* **2013**, *5*, 5002–5008.

(S35) Yuan, H.; Li, J.; Yang, W.; Zhuang, Z.; Zhao, Y.; He, L.; Mai, L. Oxygen Vacancy-Determined Highly Efficient Oxygen Reduction in $NiCo_2O_4$/Hollow Carbon Spheres. *ACS Appl. Mater. Interfaces* **2018**, *10*, 16410–16417.

(S36) Li, J.; Lu, S.; Huang, H.; Liu, D.; Zhuang, Z.; Zhong, C. ZIF-67 as Continuous Self-Sacrifice Template Derived $NiCo_2O_4$/Co, N-CNTs Nanocages as Efficient Bifunctional Electrocatalysts for Rechargeable Zn-Air Batteries. *ACS Sustainable Chem. Eng.* **2018**, *6*, 10021–10029.